Suspended honeycomb nanowire ISFETs for improved stiction-free performance

2014 Nanotechnology 25 345501

(http://iopscience.iop.org/0957-4484/25/34/345501)

IOP Publishing Nanotechnology
Nanotechnology **25** (2014) 345501 (7pp) doi:10.1088/0957-4484/25/34/345501

Suspended honeycomb nanowire ISFETs for improved stiction-free performance

Kihyun Kim[1], Taiuk Rim[2], Chanoh Park[3], Donghoon Kim[1], M Meyyappan[2,4] and Jeong-Soo Lee[1,3]

[1] Department of Electrical Engineering, Pohang University of Science and Technology (POSTECH), Pohang, Republic of Korea
[2] Department of Creative IT Engineering and Future IT Innovation Lab, Pohang University of Science and Technology (POSTECH), Pohang, Republic of Korea
[3] Division of IT Convergence Engineering, Pohang University of Science and Technology (POSTECH), Pohang, Republic of Korea
[4] NASA Ames Research Center, Moffett Field, CA, 94035, USA

E-mail: ljs6951@postech.ac.kr

Received 7 May 2014, revised 11 June 2014
Accepted for publication 19 June 2014
Published 5 August 2014

Abstract

This paper reports high performance ion-sensitive field-effect transistors (ISFETs) with a suspended honeycomb nanowire (SHNW) structure. The SHNW can provide a longer, stiction-free channel than that which is possible with a suspended straight nanowire (SSNW) for the realization of gate-all-around biosensors. Devices with SHNWs, SSNWs and conventional nanowires on the substrate have been fabricated using a top-down approach in order to compare their electrical performances. The SHNW devices exhibit excellent electrical characteristics such as lower subthreshold swing, higher transconductance and higher linear drain current. In addition, the SHNW ISFETs show better pH sensitivity than other ISFETs. Based on the results, the SHNW device appears promising for enhancing the intrinsic performance and ensuring the reliable operation of biosensor applications.

Keywords: ion-sensitive field effect transistor, gate-all-around (GAA), honeycomb structure, stiction, pH sensing, top-down, suspended nanowire

(Some figures may appear in colour only in the online journal)

1. Introduction

Ion-sensitive field-effect transistors (ISFETs) have attracted much attention due to their potential for label-free detection and real-time response [1–3]. The nanowire form of silicon, instead of the conventional thin film, has been exploited for the ISFET channel in order to improve the intrinsic electrical characteristics [4, 5]. The development of highly sensitive ISFETs is necessary for the evolution of genomics [6], biomedical diagnostics [7], environmental monitoring [8] and drug discovery [9]. Recently, a honeycomb nanowire structure has been investigated in order to provide enhanced electrical and mechanical properties for nanodevices [10]. The sensitivity of ISFETs is mainly related to intrinsic electrical characteristics in terms of transconductance (g_m) and subthreshold swing (*SS*). The gate-all-around (GAA) structure, using nanowire channels, has been demonstrated in CMOS technology and has shown superior gate controllability [11, 12]. The suspended nanowire structures with a long channel length and a low channel doping level have provided higher sensitivity due to an increased sensing area and the relaxation of the diffusion constraints of a surface bound nanowire [13–15].

In spite of the above advantages, a liquid-based operation and environment can cause the suspended nanowires to collapse and stick together which is known as stiction. This can happen, for example, during fabrication steps, such as wet etching and wet cleaning steps, or during the characterization. Stiction is a critical issue in the suspended nanostructures because it can degrade the device's performance [16]. For a given diameter, the nanowires cannot be arbitrarily long without suffering stiction and other mechanical stability problems.

In this work, we compare the intrinsic performance and the pH response of ISFETs that were fabricated using three types of nanowire structures: the suspended honeycomb nanowire (SHNW), the suspended straight nanowire (SSNW) and the conventional nanowire (CNW), which is the case with straight nanowires on the substrate. To investigate the superior stiction resistance of the SHNW, the maximum stiction-free length (L_{Max}) is extracted for different widths of the nanowires.

2. Experimental details

2.1. Investigation of stiction

The suspended nanowires (the SHNW and the SSNW) with various widths and lengths were formed on a silicon-on-insulator (SOI) wafer. Electron-beam lithography (EBL) and inductively-coupled plasma reactive ion etching (ICP-RIE) were used to fabricate the honeycomb nanowire and the 20-parallel straight nanowire structures. The width of the nanowires varied from 30 to 100 nm, and the length of the nanowires varied from 1 to 10 μm. The thickness of the nanowire was fixed at 100 nm. The nanowires were released from the substrate using diluted HF. The gap between the nanowires and the substrate was fixed at 130 nm. Then, the suspended nanowires were rinsed by de-ionized water and dried by nitrogen. Scanning electron microscopy (SEM) and transmission electron microscopy (TEM) were used to examine the occurrence of stiction.

2.2. Device fabrication

A 6-inch SOI wafer (p type, ~10 $\Omega \cdot$cm, (100)) with a top-Si layer of 100 nm and a buried oxide (BOX) layer of 200 nm was used as the substrate. First, the active area, including the channel region and the source/drain region, was formed using photolithography and ICP-RIE. Then, arsenic ions with a dose of 5×10^{15} cm^{-2} were implanted into the source and drain regions. Subsequently, rapid thermal annealing at 1000 °C for 20 s was performed, and then the nanowire structures were fabricated using EBL and ICP-RIE with a mixture of HBr, Cl_2 and O_2. Although the ICP-RIE has advantages that help to define nanowires with a narrow width, it may cause plasma-induced traps on the nanowire surface, which may degrade the electrical characteristics and affect the detection sensitivity [17–19]. In order to remove the etch damage on the nanowire's surface, a 5 nm-thick sacrificial oxide was grown using a furnace, followed by a diluted HF dip to etch the sacrificial oxide. Before the gate oxidation, the SHNW and the SSNW were released from the BOX using a diluted HF etchant. Then, a 5 nm-thick SiO_2, to serve as a sensing membrane, was grown using a furnace at 850 °C. Next, 20 nm Ti and 200 nm Ag layers were deposited and patterned using a conventional lift-off process for the source/drain contact pads and the pseudo-Reference electrode (pRE).

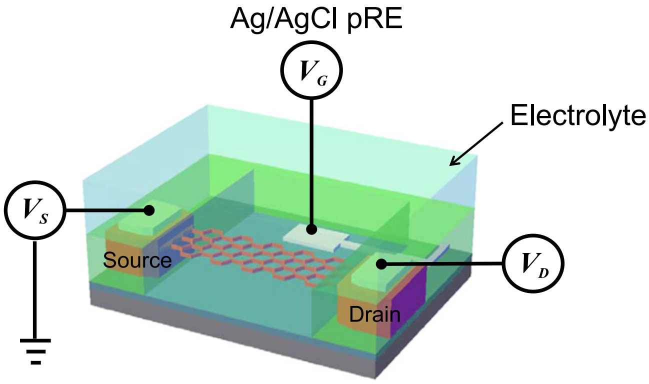

Figure 1. Schematic of the characterization setup for measuring the electrical performance and the pH response. The gate voltage (V_G) is applied to the embedded Ag/AgCl pseudo-reference electrode (pRE) immersed in the 10 mM phosphate buffered saline (PBS, pH 7.4). The drain is connected to the constant voltage ($V_D = 0.1$ V) and to a source-to-ground connection.

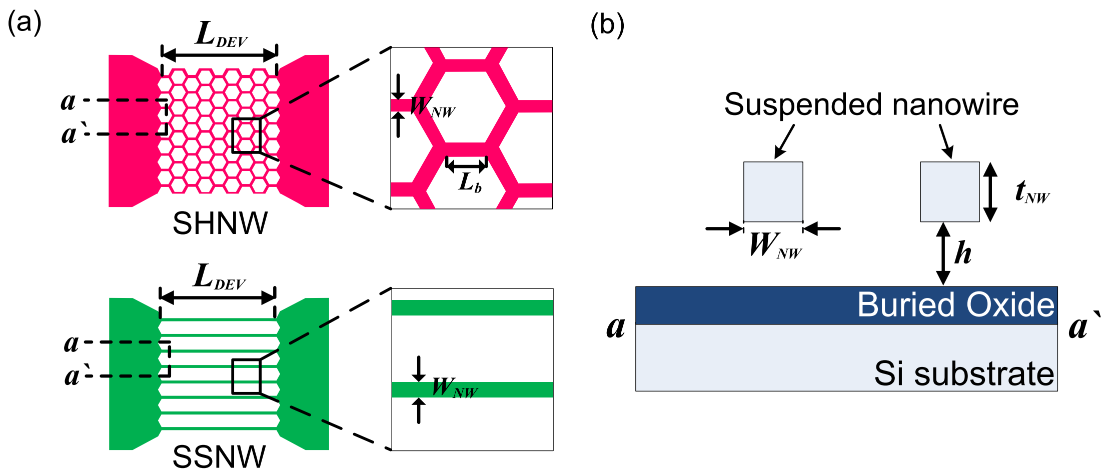

Figure 2. Schematic of the suspended honeycomb nanowire (SHNW) and the suspended straight nanowire (SSNW). (a) A schematic of the top-view. (b) A schematic of the cross-view. The parameters (h, t_{NW}, W_{NW}, L_{DEV} and L_b) are defined.

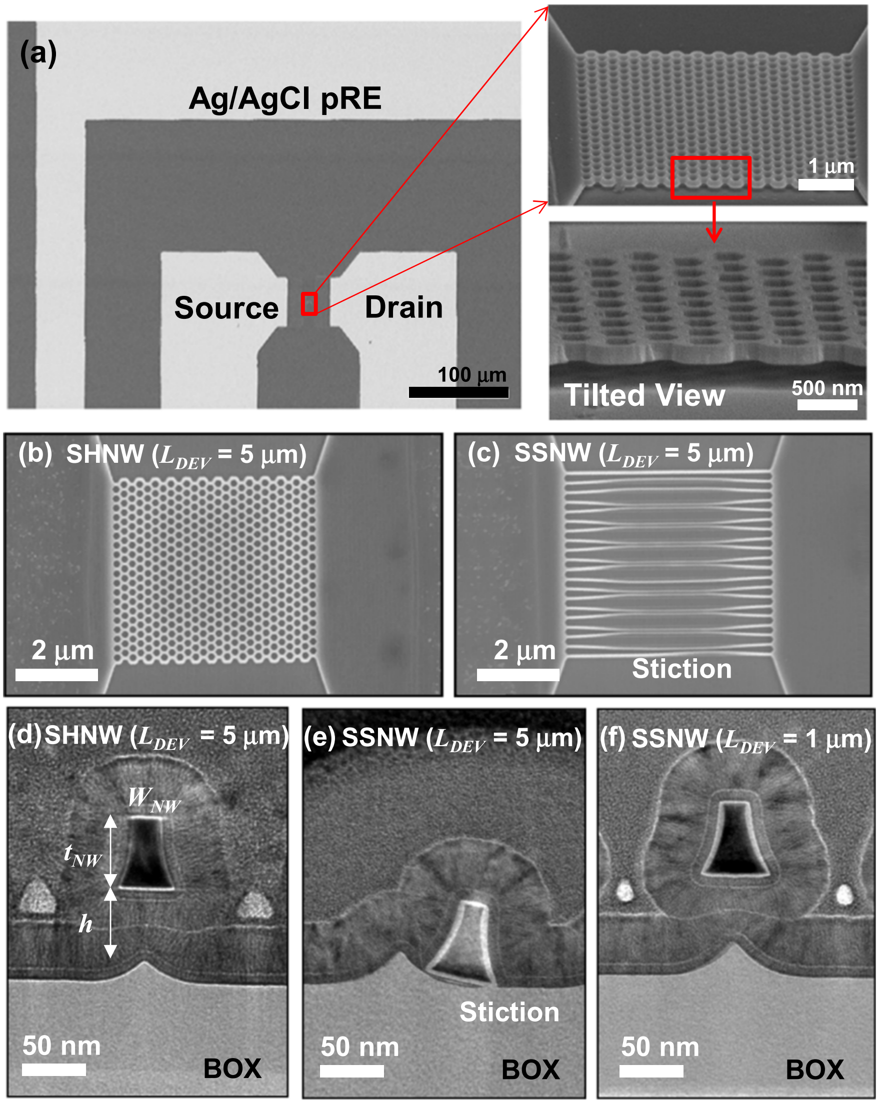

Figure 3. SEM and cross-sectional TEM images of fabricated devices. (a) SEM top-side view of the entire SHNW device with source, drain and pRE. Close-up tilted SEM images of the SHNW (b) and (c) SEM images of the SHNW and the SSNW ISFETs, respectively ($L_{DEV} = 5\ \mu$m). (d)–(f) TEM images of the SHNW with $L_{DEV} = 5\ \mu$m and of the SSNW with $L_{DEV} = 5\ \mu$m and $L_{DEV} = 1\ \mu$m.

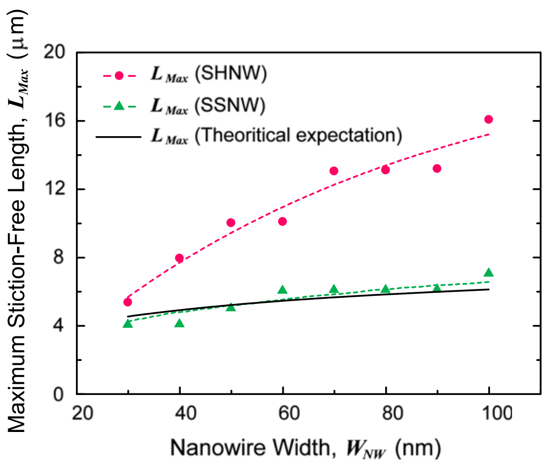

Figure 4. Maximum stiction-free length (L_{Max}) graph of the SHNW and the SSNW as a function of the nanowire width. The theoretical value for a single nanowire is calculated from the elastocapillary equation. The measured L_{Max} of the SHNW is 1.3–2.5 times longer than that of the SSNW for various nanowire widths.

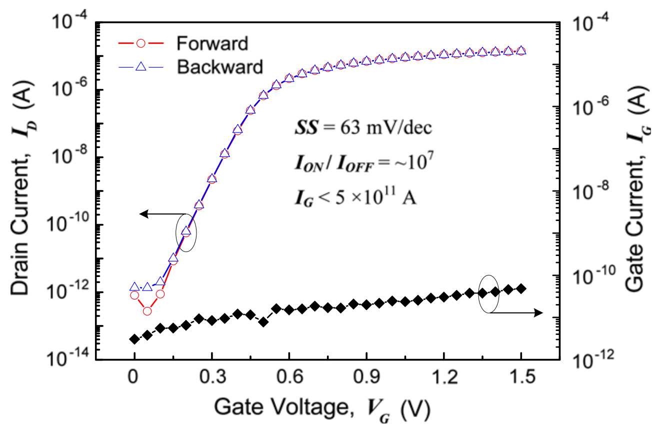

Figure 5. The I_D–V_G curve (left axis) and the I_G–V_G curve (right axis) of a SHNW ISFET at a constant V_D. The device exhibits a high on-off I_D ratio of 10^7, negligible hysteresis and a I_G of less than 5×10^{-11} A.

A 2 μm-thick SU-8 layer was coated over the wafer, except the sensing area and the pRE, in order to prevent leakage paths through the aqueous solution. Finally, the Ag/AgCl pRE was formed using an electrochemical method. The electrical potential fluctuation of the embedded Ag/AgCl pRE was previously reported to be invariant during a pH sensing measurement [20]. The CNW ISFETs were fabricated using the same process mentioned above, except for the wet etching step used to release the nanowires from the substrate.

2.3. Electrical measurements

Figure 1 is a schematic of the measurement setup for characterizing the electrical performance and the pH sensitivity. The electrical characteristics were measured using a semiconductor parameter analyzer (Keithley 4200) at room temperature. The 10 mM phosphate buffered saline (PBS, pH 7.4) was used as the electrolyte, and a gate voltage (V_G) was applied to the embedded Ag/AgCl pRE. To obtain the electrical characteristics of the devices, the drain current (I_D) and the gate current (I_G) were measured while sweeping the V_G from 0 to 1.5 V at constant drain voltage ($V_D = 0.1$ V) and source voltage ($V_S = 0$ V). Various pH solutions from 4 to 10 were prepared by adding 1.2 M HCl and 1 M NaOH solution to 10 mM PBS in order to demonstrate the pH sensitivity of the fabricated devices.

3. Results and discussion

The suspended nanostructure can suffer from a stiction problem, which can distort the crystalline active region and thus jeopardize reliable operation. Stiction problems mainly arise from the vaporization of the aqueous solution used in processing or during operation, which is inevitable. The volume of liquid among the suspended nanowires and the substrate can shrink due to liquid vaporization. The capillary forces, the van der Waals forces, the electrostatic attraction and the hydrogen bridging become larger than the restoring force as the volume decreases, resulting in the distortion of the suspended nanowire. Among the forces, the capillary force plays a dominant role in the stiction problem. Hence, an elastocapillary number (N_{EC}), which defines the ratio of elastic restoring energy to the capillary energy, is considered to forecast the stiction of a suspended structure according to width [21]. The N_{EC} is given by

$$N_{EC} = \frac{128Eh^2 t_{NW}{}^3}{15\gamma_l \cos\theta_c L_{DEV}{}^4 \left(1 + \dfrac{t_{NW}}{W_{NW}}\right)} \times \left[1 + \frac{2\sigma_r L_{DEV}{}^2}{7Et_{NW}{}^2} + \frac{108h^2}{245t_{NW}{}^2}\right] \quad (1)$$

where Young's modulus (E), the gap between the nanowire and the substrate (h), the thickness of the nanowire (t_{NW}), the liquid surface tension (γ_l), the contact angle (θ_c), the residual tensile (σ_r), the width of the nanowire (W_{NW}) and the length of the nanowire (L_{DEV}) are involved in determining stiction.

The stiction problem can easily occur when the surface of a suspended object has an oxide layer (>5 Å) that is related with θ_c and σ_r. The oxide surface, which has a high surface energy with the hydroxyl groups, is extremely hydrophilic, and a strong capillary force between the suspended objects develops as the aqueous solution is vaporized [22]. Therefore, the FET-based sensors that contain the surface hydroxyl group are vulnerable to the stiction problem. According to equation (1), the stiction issue can be mitigated as the width of the nanowire increases. However, the width of the nanowire cannot be enlarged for the sensor application because the sensitivity is directly related to the width of the nanowire. The parameters (h, t_{NW}, W_{NW} and L_{DEV}) are illustrated in figures 2(a) and (b). The branch length (L_b) of the honeycomb nanowire was 100 nm. Note that when $h = 0$, SSNW becomes CNW when directly sitting on the substrate. The stiction-free nanostructure can be obtained for $N_{EC} > 1$, whereas the suspended structures stick to the substrate for $N_{EC} < 1$.

Figure 3 shows the SEM and the TEM images of the fabricated devices. Figure 3(a) shows the SEM images of representative SHNW ISFETs with source and drain, the Ag/AgCl pRE and the suspended nanowire, revealing that the Ag/AgCl pRE is embedded near the device and the SHNW is connected between the source and the drain. The SHNW and the SSNW have the same physical dimensions ($W_{NW} = 20$ nm, $t_{NW} = 65$ nm, $h = 70$ nm, and $t_{ox} = 5$ nm), as seen in the TEM images (figures 3(d)–(f)). Whereas the SHNW ($L_{DEV} = 5$ μm) is free of stiction, the SSNW ($L_{DEV} = 5$ μm) shows a collapse in the middle of the structure, as seen in figures 3(d) and (e).

Figure 4 shows the L_{Max} as a function of the nanowire width for the SHNW and the SSNW nanostructures. The L_{Max} is a critical parameter used to evaluate the stiction characteristics. The solid line indicates the calculated L_{Max} for the SSNW structures, using equation (1) when $N_{EC} = 1$ to figure out the dependence of stiction on W_{NW}. To investigate the effect of nanowire design on stiction, the experimental L_{Max} for the SHNW and the SSNW is also presented in figure 4. It turns out that the L_{Max} of the SSNW follows the estimated value from equation (1), which confirms the validity of the elastocapillary number model for estimating the L_{Max}. When the SSNW has a shorter length than the L_{Max}, it is also free from stiction (figure 3(f)).

The honeycomb structure exhibits excellent resistance to stiction as a result of superior mechanical stability enabled by periodically repeating 'Y' junctions, and it can be improved with a shorter L_b at a fixed W_{NW} [23]. The measured L_{Max} of the suspended honeycomb nanowire is 1.3–2.5 times longer than that of the SSNW for various nanowire widths, indicating superior mechanical stability. Thus, the suspended honeycomb structure with the longer L_{Max} can provide higher sensitivity and more reliable operation in biosensor applications under the same dimensions (h, t_{NW} and W_{NW}), compared to other structures.

Figure 5 shows the I_D and the I_G as a function of the V_G of a SHNW ISFET ($W_{NW} = 20$ nm, $L_b = 100$ nm, $t_{NW} = 65$ nm and $t_{ox} = 5$ nm). The I_D–V_G was measured by double sweep to observe the hysteresis characteristics. The device exhibits typical n-type FET behavior with a high on-off I_D ratio of 10^7,

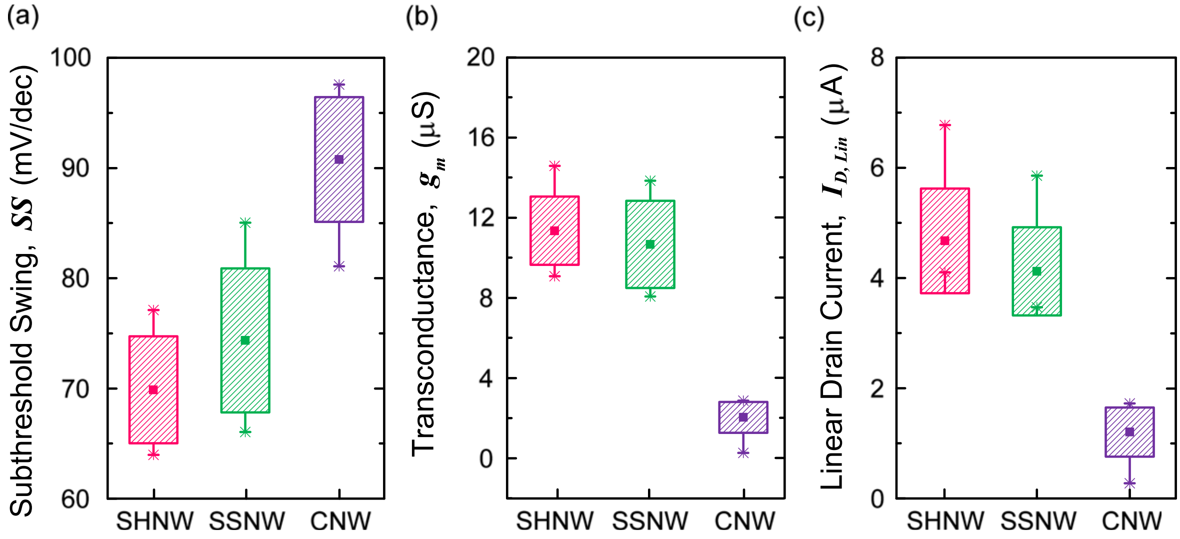

Figure 6. Electrical parameters of SHNW, SSNW and CNW ISFETs. (a) Subthreshold swing. (b) Transconductance. (c) Linear drain current. Symbols: the minimum and maximum value(⋇), the average (■) and the standard deviation (▨).

negligible hysteresis and an I_G of less than 5×10^{-11} A. The negligible hysteresis of these SHNW ISFETs means that the devices have negligible interface trap density [17, 19]. Low gate leakage current indicates that the SU-8 layer successfully prevents the leakage current flow between the Ag/AgCl pRE and the source/drain electrode through the aqueous solution.

Figure 6 shows the average value and the standard deviation of the electrical parameters, including *SS*, g_m and the linear drain current ($I_{D,Lin}$), from the fabricated devices. The parameters were extracted from eight devices in each category of SHNW, SSNW and CNW. The *SS* (=$dV_G/d\log I_D$) was extracted when the I_D was in the range of 1 nA to 10 nA. The g_m (=dI_D/dV_G) and $I_{D,Lin}$ were extracted at a gate overdrive voltage ($V_{OD} = V_G - V_{TH}$) of 0.5 V. The whole set of electrical parameters are enhanced in the increasing order of the CNW, the SSNW and the SHNW ISFETs. The best recordable *SS* of 63 mV dec^{-1} is obtained for the SHNW ISFETs, which is close to the ideal value. This value is lower than the previously reported values of *SS* for Si-nanowire FET using liquid gating (80 ∼ 150 mV dec^{-1}) [7, 10, 20, 24]. The electrical performance enhancement of SHNW devices comes from geometrical benefits of the suspended honeycomb structure such as outstanding gate controllability and enlarged surface area [10]. The honeycomb nanowire, owing to its network nature, can always provide a larger surface area than the straight nanowire array, which is an important advantage in detecting a low concentration of biomolecules and chemicals.

Figure 7(a) shows the I_D–V_G curves of the SHNW ISFETs in response to varying pH values ranging from 4 to 10. The transfer curves are shifted toward the lower V_G without any change of the *SS* and the g_m as the hydrogen ion concentration within the solution increases. To investigate the V_G shift dependence on the pH value in the subthreshold regime, the sensing voltage (V_{Sen}) is defined as the V_G at the $I_D = 1$ nA. The shift of V_{Sen} per pH ($\Delta V_{Sen}/\Delta$pH) is calculated as high as 35 mV pH^{-1} for all three types of devices, comparable with other ISFETs using a SiO_2 sensing surface with a value of 30 ∼ 40 mV pH^{-1} [10, 20, 24]. The $\Delta V/\Delta$pH is dominantly ascribed to the density of the hydroxyl groups on the sensing surface [25, 26].

The sensitivity (S) is typically defined as the absolute I_D change divided by the initial reference I_D level ($S = |\Delta I_D|/I_{D0}$), where $\Delta I_D = I_{D1} - I_{D0}$ is the drain current difference, I_{D1} is the drain current induced by the sensing event (the attachment of ions on the sensing membrane) and I_{D0} is the baseline current [27–29]. The current sensitivity is an important parameter for smart sensor applications because read-out circuits based on a current-sensing technique can operate in low voltage and at high speed [30–32]. The $I_{D0,Sub}$ is measured at $V_G = V_{Sen}$ in a pH 10 solution in the subthreshold regime, and the $I_{D0,Lin}$ is measured at $V_{OD} = 0.5$ V in a pH 10 solution in the linear regime. The baseline current is determined at pH 10 because the number of the hydrogen ions within the solution is the least at pH 10. Figures 7(b) and (c) show the average sensitivity for the fabricated ISFETs as a function of the pH value in both the subthreshold regime ($V_G = V_{Sen}$) and the linear regime ($V_{OD} = 0.5$ V). Whereas the S increases exponentially in the subthreshold regime as the hydrogen ion concentration increases, the S varies linearly in the linear regime as the hydrogen ion concentration increases. This result comes from the operation mechanism of the ISFETs, which is in fact nothing other than a MOSFET. In the MOSFET device, when V_D is a small constant, the dependence of I_D on V_G is given by [33, 34]

$$I_D \propto \exp\left(\frac{2.3V_G}{SS}\right) \quad \text{(subthreshold regime)} \qquad (2)$$

$$I_D \propto g_m\left(V_G - V_{TH}\right) \quad \text{(linear regime).} \qquad (3)$$

In the subthreshold regime, the S of the SHNW ISFETs is 5 times larger than that of the CNW ISFETs at the pH 4 condition. In the linear regime, the S_{pH} (=dS/dpH) is calculated as 0.4/pH, 0.3/pH and 0.15/pH for SHNW, SSNW and

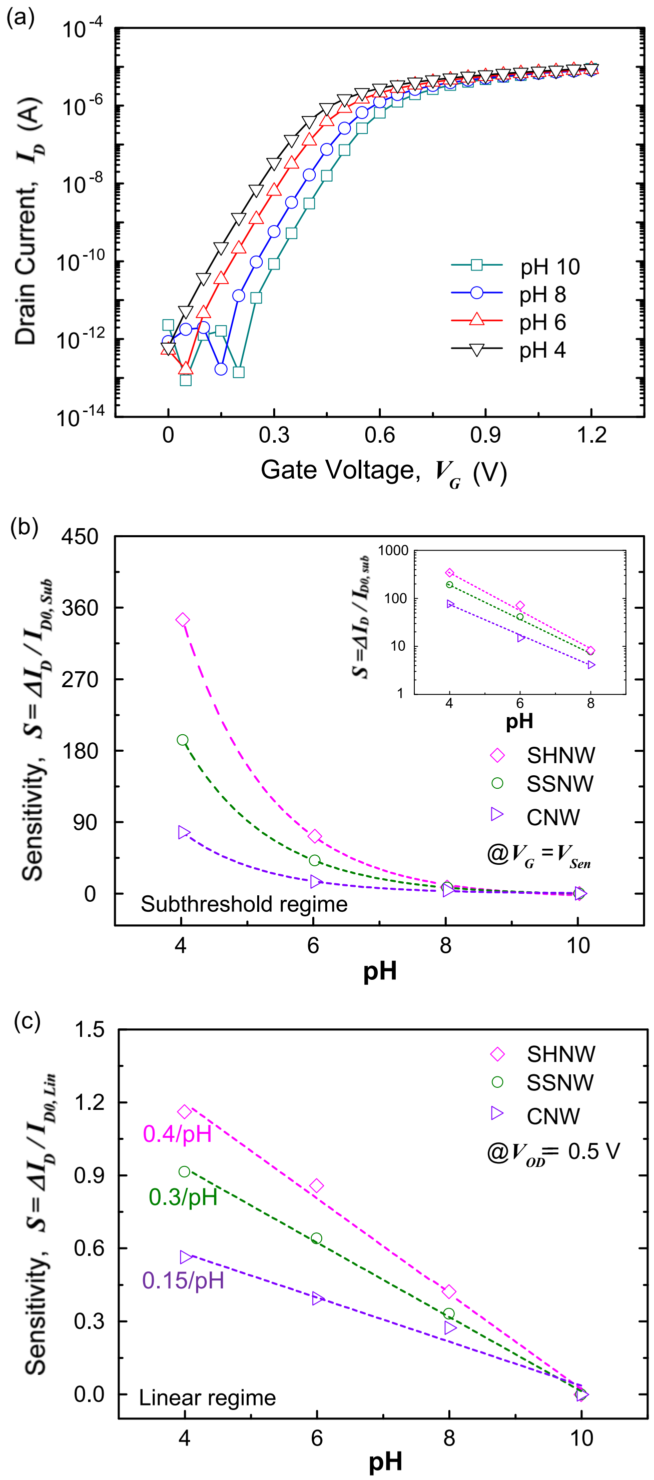

Figure 7. pH responses of SHNW, SSNW and CNW ISFETs. (a) The I_D–V_G curve shift of the SHNW ISFETs with varying hydrogen ion concentrations. (b) Average sensitivity in the subthreshold regime. Inset: average sensitivity (log scale) versus pH value. (c) Average sensitivity in the linear regime.

CNW ISFETs, respectively. The SHNW devices show excellent pH sensing responses both in subthreshold and linear regimes. Here, the higher sensitivity of the SHNW devices results from a lower *SS* in the subthreshold regime and a higher g_m in the linear regime of SHNW, which can generate larger ΔI_D with the same amount of surface charges (which is induced by hydrogen ions bound to the SiO_2 surface) at a given gate bias (equations (2) and (3)). Consequently, the SHNW ISFETs show higher pH sensitivity than other devices due to improved electrical characteristics.

4. Conclusions

We have demonstrated a suspended honeycomb nanowire structure for the gate-all-around ISFETs with a high immunity to stiction, better intrinsic characteristics and a higher pH sensitivity. In order to compare the stiction immunity and the intrinsic characteristics for various nanowire dimensions, honeycomb nanostructures and other straight nanowire structures were fabricated, characterized and compared at room temperature. The honeycomb devices can provide a longer L_{Max} with the nanowire width in the range of 30–100 nm and a large sensing area without the stiction problem. It can provide a L_{Max} up to 2.5 times longer than the conventional nanowire structures, depending on the nanowire width. The honeycomb devices exhibit improved electrical characteristics in terms of *SS*, g_m and $I_{D,Lin}$, which are attributed to geometrical benefits such as better gate controllability and increased effective channel width. In addition, the honeycomb devices exhibit better pH sensitivity, mainly due to a smaller *SS* value and a larger g_m. Therefore, the suspended honeycomb nanostructure is very promising as an advanced sensor platform for label-free, real-time detection of biomolecules.

Acknowledgment

This work was in part supported by the National Research Foundation (NRF) (No. 2013R1A1A2007094), by a grant (Code No. 2011-0031638) from the center for advanced soft electronics under the global frontier research program of the Ministry of Education, Science, and Technology (MEST) and by the 'IT Consilience Creative Program' (NIPA-2014-H0201-14-1001) supervised by the National IT Industry Promotion Agency, Korea.

References

[1] Bergveld P 2003 *Sensors Actuators* B **88** 1
[2] Bergveld P 1986 *Biosens.* **2** 15
[3] Poghossian A, Cherstvy A, Ingebrandt S, Offenhäusserb A and Schöning M J 2005 *Sensors Actuators* B **111** 470
[4] Cui Y, Wei Q, Park H and Lieber C M 2001 *Science* **293** 1289
[5] Grieshaber D, MacKenzie R, Voros J and Reimhult E 2008 *Sensors* **8** 1400
[6] Hahm J and Lieber C M 2004 *Nano Lett.* **4** 51
[7] Stern E, Klemic J F, Routenberg D A, Wyrembak P N, Turner-Evans D B, Hamilton A D, LaVan D A, Fahmy T M and Reed M A 2007 *Nature* **445** 519
[8] Frost R R and Griffin R A 1977 *Soil Sci. Soc. Am. J.* **41** 53
[9] Baumann W H, Lehmann M, Schwinde A, Ehret R, Brischwein M and Wolf B 1999 *Sensors Actuators* B **55** 77

[10] Rim T, Kim K, Kim S, Beak C-K, Meyyappan M, Jeong Y-H and Lee J-S 2013 *IEEE Electron Device Lett.* **34** 1059
[11] Singh N *et al* 2006 *IEEE Electron Device Lett.* **27** 383
[12] Ng H T, Han J, Yamada T, Nguyen P, Chen Y P and Meyyappan M 2004 *Nano Lett.* **4** 1247
[13] Kim D R and Zheng X 2008 *Nano Lett.* **8** 3233
[14] Roy S and Gao Z 2009 *Nano Today* **4** 318
[15] Kim A, Ah C S, Yu H Y, Yang J-H and Baek I-B 2007 *Appl. Phys. Lett.* **91** 103901
[16] Han J-W, Moon D-I and Choi Y-G 2009 *IEEE Electron Device Lett.* **30** 864
[17] Stern E, Klemic J F, Routenberg D A, Wyrembak P N, Turner-Evans D B, Hamilton A D, LaVan D A, Fahmy T M and Reed M A 2007 *Nature* **445** 519
[18] Li Z, Chen Y, Li X, Kamins T I, Nauka K and Williams R S 2004 *Nano Lett.* **4** 245
[19] Eriguchi K, Matsuda A, Takao Y and Ono K 2014 *Japan J. Appl. Phys.* **53** 03DE02
[20] Rim T, Kim K, Hong N, Ko W, Baek C-K, Jeon S, Deen M J, Meyyappan M, Jeong Y-H and Lee J-S 2013 *RSC Advances* **3** 7963
[21] Mastrangelo C H and Hsu C H 1993 *J. Microelectromech. Syst.* **2** 33
[22] Maboudian R and Howe R T 1997 *J. Vac. Sci. Tech.* **15** 1
[23] Sun Y, Chen Q and Pugno N 2014 *Compos. Struct.* **107** 698
[24] Kim S, Rim T, Kim K, Lee U, Baek E, Lee H, Baek C-K, Meyyappan M, Deen M J and Lee J-S 2011 *Analyst* **136** 5012
[25] Bousse L, Rooij N F D and Bergveld P 1983 *IEEE Trans. Electron Devices* **30** 1263
[26] Bousse L, Rooij N F D and Bergveld P 1983 *Surf. Sci.* **135** 479
[27] Gao A, Lu N, Wang Y, Dai P, Li T, Gao X, Wang Y and Fan C 2012 *Nano Lett.* **12** 5262
[28] Shin K S, Pan A and Chui C O 2012 *Appl. Phys. Lett.* **100** 123504
[29] Park C W, Ahn C G, Yang J H, Baek I B, Ah C S, Kim A S, Kim T Y and Sung G Y 2009 *Nanotechnology* **20** 475–501
[30] Seevinck E, van Beers P J and Ontrop H 1991 *IEEE J. Solid-State Circuits* **26** 525
[31] Zhang M, Haider M R, Huque M A, Adeeb M A, Rahman S and Islam S K 2007 *Smart Mater. Struct.* **16** 525
[32] Zhang L, Yu Z and He X 2009 *IEEE Trans. on Circuits and Systems* **56** 540
[33] Streetman B G and Banerjee S K 2006 *Solid State Electronic Devices* 6th edn (Upper Saddle River, NJ: Pearson Education) chapter 6
[34] Neamen D A 2007 *Semiconductor Physics and Devices: Basic Principles* 3rd edn (New York: McGraw-Hill) chapter 11